

Modeling roughness surface R_p of 3D selective laser melting metal materials

Matej Babič^{1*}, Roman Šturm², Peter Horňák³

¹*Faculty of Information Studies, Novo Mesto, Slovenia*

²*Faculty of Mechanical Engineering, Ljubljana, Slovenia*

³*Faculty of Materials, Metallurgy and Recycling, Technical University of Košice, Slovak Republic*

Received 1 March 2024, received in revised form 23 August 2024, accepted 6 September 2024

Abstract

A part's surface layer quality is dictated by several factors, including surface roughness, the microstructure of the metal surface layer, and the part's mechanical and physical state. The operating characteristics of machine components, such as wear resistance, vibration resistance, contact strength, connection strength, part strength under cyclic loads, etc., are influenced by surface layer conditions. The part's surface roughness is just one of the primary geometric attributes of a part's quality, which is its accuracy in terms of size and shape. The current work models the roughness surface of 3D selective laser melting of metal materials using genetic programming and multiple regression. It then explains how to measure surface roughness using this method. A novel approach to pattern recognition for analyzing the roughness of metal materials melted using a 3D selective laser is introduced. Fractal geometry determines the complexity of 3D selective laser melting of metal materials.

Key words: 3D selective melting, graph theory, pattern recognition, genetic programming, multiple regression

1. Introduction

In recent years, 3D printing technology has grown rapidly [1]. 3D printing is based on three-dimensional digital representation. This manufacturing method prints an object by dividing it into layers. This printing process uses a variety of materials and inks. Metal powder 3D printing has made rapid progress over the past ten years. At the same time, with the development of the industry, many myths and misconceptions have appeared. Additive manufacturing of metal products will boost sales of CNC machines and other traditional parts machining tools. The future factory will include many production technologies. The challenge for product development engineers will be to know when to use a particular technology to provide the most value to the product. Additive manufacturing is suitable for creating complex products that cannot be made traditionally. Increasing complexity does not add significant costs to modeling the part on the machine. However, this statement does not consider the

additional development or post-processing time. It is unprofitable to produce products of simple geometry on a metal 3D printer. Metal printers are designed to solve much more complex problems. 3D metal printing is the additive manufacturing of metal products, rightfully one of the most promising and rapidly developing areas of 3D printing. The technology dates back to the conventional sintering of materials used in powder metallurgy. But now, it has become more advanced, accurate, and faster.

Selective laser melting (SLM) [2] is an additive manufacturing or 3D printing technique that uses lasers to fuse metal powder into solid 3D objects. SLM is suitable for processing reactive high-strength metals, such as titanium, aluminum, stainless steel, cobalt chromium, and nickel alloys, into functionally dense parts with complex geometries. SLM is an innovative technology for manufacturing complex in-shape and structure products from metal powders using mathematical CAD models. This process consists of sequential layer-by-layer melting of powder material using

*Corresponding author: e-mail address: babicster@gmail.com

powerful laser radiation. SLM opens the broadest opportunities for modern production because it allows you to create metal products of high precision and density, optimize the design, and reduce the weight of manufactured parts. Using SLM, it is feasible to produce items with better mechanical and physical qualities than those made with conventional technology. As SLM technology allows for the management of product qualities, it is feasible to build unique, complex-profile items without the need for machining or expensive equipment. SLM machines are designed to solve complex problems in aerospace, energy, oil and gas, mechanical engineering, metalworking, medicine, and jewelry. They are also used in research centers, design bureaus, and educational institutions when conducting research and experimental work.

Why is geometry perceived as “dry” and “cold”? Its inability to characterize the form of a cloud, mountain, tree, or coastline is one of the causes. Tree bark cannot be described as smooth. Clouds cannot be described as spheres. Mountains cannot be described as cones. Circles cannot represent coastlines, and lightning cannot follow a straight route. More broadly, I say that many of Nature’s forms are so uneven and fragmented that Nature shows only a higher degree of complexity – not a whole different level – than Euclidean figures. For any practical problem, quantity-different length scales in natural forms can be considered limitless. Such phenomena present us with challenges and motivate us to do additional in-depth research by examining the forms that Euclid rejected due to their “formlessness” – that is, by investigating the morphology of the “amorphous.” This problem was disregarded by mathematicians, who instead chose to create a myriad of theories that do not begin to explain the things perceived or experienced. I took a chance to rise to the challenge and created a new geometry of nature with applications across various domains. The new geometry defines a family of figures I call fractals [3] and can depict many asymmetrical and fragmented patterns around us. It can also give rise to fully developed theories.

Graphs or networks [4] are an important mathematical tool that allows you to model and analyze various systems and relationships between objects. A graph is an abstract mathematical structure consisting of vertices (nodes) and edges (links) between these vertices. Graphs are widely used to model and analyze various systems and relationships. In a graph, each vertex represents an individual element or object, and the edges represent connections or relationships between those elements. For example, in a social connection graph, each vertex could represent an individual, and the edges could represent friendship or acquaintance between people. Graphs are an important tool in graph theory and have a wide range of applications in various fields, such as computer sci-



Fig. 1. EOS M 290.

ence, transportation logistics, social networks, biology, material science, and others.

Pattern recognition [5] is the process of extracting source data from the total mass of heterogeneous objects and classifying them according to characteristic features. These are powerful technologies that are widely used in almost all industries today. Pattern recognition plays an important role in modern information systems. Automatic image recognition systems have become especially widespread. Despite the widespread commercialization of the software market, the research intensity in this area does not decrease because the reliability of existing solutions is still insufficient. The problem is especially aggravated if the database consists of thousands of standards, leading to the complication of models of classified objects and, consequently, the impossibility of implementing existing algorithms in real time.

This study aims to present a new pattern recognition method for characterizing roughness R_p of 3D selective laser melting of metal materials.

2. Material preparation and experimental work, methodology

2.1. Experimental work and material preparation

Since 2014, the EOS M 290 [6] has been utilized in the serial manufacture of numerous applications. Its three predecessors’ solid and dependable performance has been built upon, guaranteeing homogeneous part qualities from machine to machine, task to job, and part to part. It is the obvious choice for flexible serial production of metal components due to its large selection of materials, extensive monitoring suite, and ease of integration into your production. Figure 1 presents EOS M 290, and the parameters of EOS M 290 are shown in Table 1.

Table 1. Parameters of EOS M 290

Construction volume	$250 \times 250 \times 325 \text{ mm}^3$ ($9.85 \times 9.85 \times 12.8 \text{ in}^3$) (height incl. build plate)
Laser type	Yb-fiber laser; 400 W
Precision optics	F-theta lens; high-speed scanner
Scan speed	up to 7.0 m s^{-1} (23 ft sec^{-1})
Focus diameter	$100 \mu\text{m}$ (0.004 in)
Power supply	32 A/400 V
Power consumption	max. 8.5 kW/average 2.4 kW/with platform heating up to 3.2 kW
Compressed air supply	7,000 hPa; $20 \text{ m}^3 \text{ h}^{-1}$ (102 psi; $706 \text{ ft}^3 \text{ h}^{-1}$)
Machine dimensions ($W \times D \times H$)	$2,500 \times 1,300 \times 2,190 \text{ mm}^3$ ($98.4 \times 51.2 \times 86.2 \text{ in}^3$)
Recommended installation space	min. $4,800 \times 3,600 \times 2,900 \text{ mm}^3$ ($189 \times 142 \times 114 \text{ in}^3$)
Weight	approx. 1,250 kg (2,756 lb)
Software	<i>EOSPRINT</i> incl. <i>EOS ParameterEditor</i> , <i>EOSTATE Everywhere</i> , <i>EOSCONNECT Core</i> , <i>EOSCONNECT MachinePark</i> , <i>Materialise Magics Metal Package and modules</i>

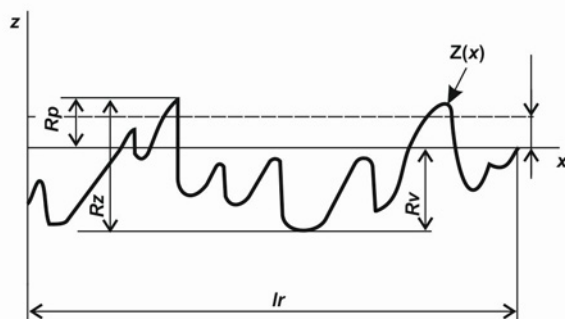


Fig. 2. Surface roughness profile.

Material EOS Maraging Steel MS1 is used. Tool steel powder used for EOS DMLSTM systems processing is called EOS Maraging Steel MS1. The chemical composition of parts constructed in EOS Maraging Steel MS1 complies with US classification 18 % Ni Maraging 300, European 1.2709, and German X3NiCoMoTi 18-9-5. The steel powder known as Maraging Steel (MS1) is distinguished by its strength and toughness. After construction, parts can be easily machined and post-hardened at temperatures above 50 HRC. This material is perfect for high-performance industrial and engineering parts, such as those used in motor racing and aerospace, and for various tooling applications, including injection molding, die casting of light metal alloys, punching, extrusion, etc.

Roughness [7] is a set of surface irregularities with relatively small steps identified using the base length. Irregularities with large steps are referred to as waviness, and with very large steps – as deviations in shape. Surface roughness significantly affects the gaps and tensions in joints, the strength of parts under variable loads, wear resistance, corrosion resistance, tightness, and other performance characteristics of parts. Maximum Profile Peak Height: R_p is the distance be-

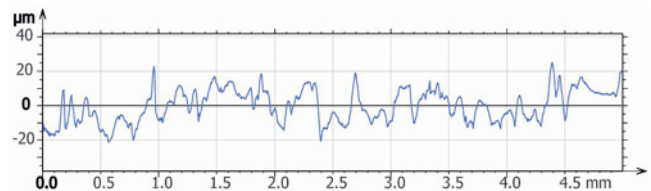
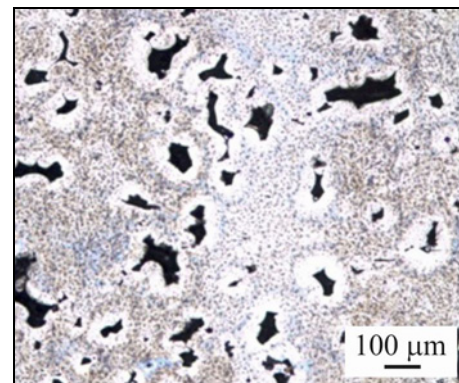
Fig. 3. Roughness R_p of SLM specimen.

Fig. 4. Microstructure of SLM specimen.

tween the highest point of the profile and the mean line within the evaluation length. Figure 2 presents the surface roughness profile. Figure 3 presents the roughness R_p of the SLM specimen, and Fig. 4 presents the microstructure of the SLM specimen.

2.2. Methodology

The microstructure of the SLM specimen is very complex. Classical Euclidian geometry cannot be used. Fractal geometry has to be used to characterize the complexity of the microstructure of the SLM specimen.

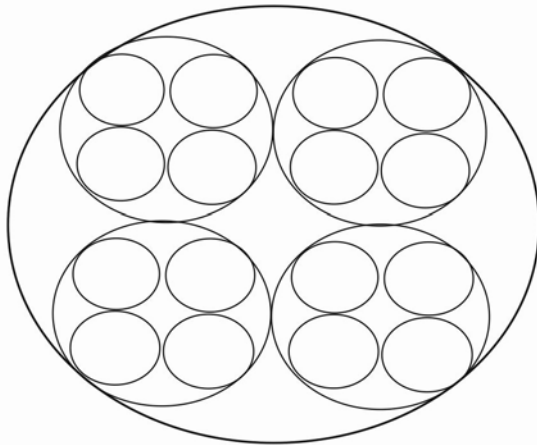


Fig. 5. Homeomorphic fractal model.

2.2.1. Fractals

Two things are important in fractal geometry: self-similarity or self-affinity and fractal dimension. In this research, the homomorphic fractal model is presented.

2.2.1.1. The homeomorphic fractal model

The homeomorphic fractal model [9] is based on drawing circles or ellipses with different radii. The method is suitable for black-and-white images. The largest radius $R1$ of the crust (ellipse) is chosen. With it, the black dots can still be covered. Then, a smaller radius $R2$ is chosen, and the process is continued. Count the number of circles (ellipses) with the same radii. The fractal dimension is represented by the directional coefficient of the graph line of $\log(\text{radius size})$ and $\log(\text{number of circles/ellipses})$. Fractal patterns are used to describe the complexity of the microstructure of SLM materials. Fractional dimensions are a measure of fractal complexity that shows how much the objects occupy the available space. Without regard to integer values, the fractal dimension quantifies the shift in the “size” of a fractal set as the observational scale changes. Figure 5 presents a

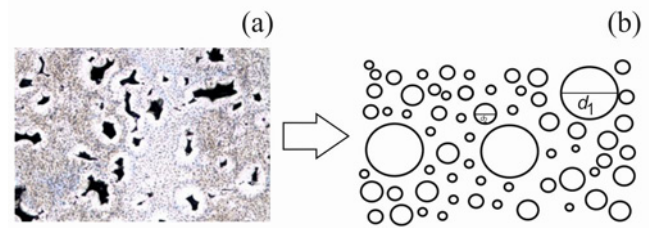


Fig. 6. Microstructure of SLM and homeomorphic fractal model, drawing circles with different radii.

homeomorphic fractal model. Figure 6 presents the microstructure of SLM and the homeomorphic fractal model, drawing circles with different radii.

2.2.2. Pattern recognition

A novel method for pattern identification using network theory was created. Firstly, the homeomorphic fractal model is used. Each circle is connected with the circle with an equal radius d_1 (Fig. 7b). Then, connections are transformed into networks (Fig. 7c). For this graph, density is calculated:

$$\eta = 2 \times E/V \times (V - 1), \quad (1)$$

where V is the number of vertexes and E is the number of edges in the graph.

2.2.3. Modeling

For modeling the roughness of the surface of 3D SLM specimens, intelligent system methods (genetic programming and linear regression) are used. The automatic construction or modification of programs using genetic algorithms is known as genetic programming (GP) [10–12]. In genetic programming, the individuals in a population represent the programs. It is convenient to represent these programs as trees where functions are represented by internal nodes to which subtrees are attached as input parameters. The leaves of such a tree will be constants, task input parameters, or program directive commands. This presentation of

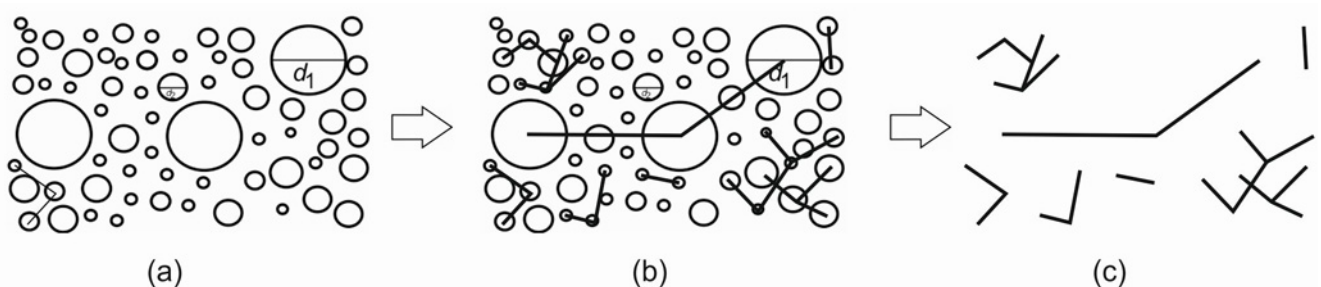


Fig. 7. A novel method for pattern recognition.

Table 2. Parameters of SLM specimen

Specimen	Power (W) X1	Speed (mm s ⁻¹) X2	FD X3	Density of network η X4
S1	320	1000	1.54	0.69
S2	320	1150	1.51	0.64
S3	320	1300	1.67	0.84
S4	270	850	1.65	0.72
S5	270	1000	1.75	0.81
S6	270	1150	1.57	0.75
S7	270	1300	1.49	0.55
S8	220	700	1.78	0.91
S9	220	850	1.84	0.49
S10	220	1000	1.56	0.72
S11	220	1150	1.76	0.70
S12	220	1300	1.83	0.37
S13	170	700	1.61	0.66
S14	170	850	1.55	0.57
S15	170	1000	1.74	0.48
S16	170	1150	1.73	0.27
S17	170	1300	1.59	0.25

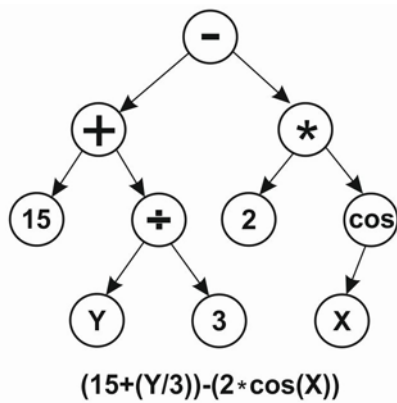


Fig. 8. Simple tree program of GP.

programs is clear and easy to implement. However, working with trees is not always convenient when performing operators, such as crossing over and mutation. Essentially, completely new operators need to be implemented. Crossing over will consist of replacing one of the subtrees of the first parent with some subtree of the second parent. A mutation will perform a random change in one of the tree nodes (for example, changing a function or constant). Thus, using trees entails several problems: creating new mutation and crossover operators and the dynamic length of the chromosome encoding the tree. Figure 8 presents a simple GP tree program.

A multiple linear regression model [13] is a practical statistical model for assessing the relationships between a continuous dependent variable and predictor variables. Predictors might be derived fields, continuous or categorical, to accommodate nonlinear relationships. As the model is made up of additive terms – each of which is a predictor multiplied by a coefficient estimate – it is linear. A constant, or free term, is also typically included in the model. Charts with at least two continuous fields – one designated as the target variable and the other as the predictor variable – can be analyzed using linear regression to identify trends. To create an appropriate regression model, such a chart can also be described with two auxiliary continuous fields and a categorical predictor:

$$Y_i = B_0 + B_1 \times x_1 + B_2 \times x_2 + \dots + B_n \times x_n + \epsilon, (2)$$

where Y_i is the dependent or predicted variable, B_0 is the y -intercept, i.e., the value of y when both x_1 and x_2 are 0, B_1 and B_2 are the regression coefficients representing the change in y relative to a one-unit change in x_{i1} and x_{i2} , respectively, B_n is the slope coefficient for each independent variable, and ϵ is the model's random error (residual) term.

3. Results and discussion

The SLM specimen's parameters are shown in Table 2. Specimens S1 to S17 are indicated in the first column. The second column shows the laser's power in W. X1 is used to indicate this parameter. The speed of the laser is shown in mm s⁻¹ in the second column. X2 is used to represent this parameter. The SLM specimen's complexity is shown in the third column. X3 is used to indicate this attribute. The density of the SLM specimen's microstructure network is represented in the fourth column. X4 is used to indicate this parameter. A hatch distance of 0.11 mm was employed. Table 3 shows the roughness of $R_p x$ and $R_p y$ of the SLM specimen. Y is expressed in μm. Roughness $R_p x$ is presented in the second column, while

Table 3. Roughness $R_p x$ and $R_p y$ of SLM specimen

Specimen	$R_p x$ (μm) Y	$R_p y$ (μm) Y
S1	19.37	21.93
S2	23.70	18.70
S3	20.93	15.13
S4	26.20	21.23
S5	21.00	17.37
S6	26.40	23.67
S7	23.23	22.47
S8	22.97	20.60
S9	19.20	22.30
S10	18.17	20.17
S11	22.53	20.20
S12	20.97	23.07
S13	21.00	18.40
S14	20.13	21.10
S15	16.77	20.57
S16	22.03	23.13
S17	20.63	17.93

$R_p y$ is presented in the final column. Specimens S1 to S17 are indicated in the first column. The second column shows the laser’s power in W. $X1$ is used to indicate this parameter. The speed of the laser is shown in mm/s in the second column. $X2$ is used to represent this parameter. The SLM specimen’s complexity is shown in the third column. $X3$ is used to indicate this attribute. The density of the SLM specimen’s microstructure network is represented in the fourth column. $X4$ is used to indicate this parameter. A hatch distance of 0.11 mm was employed. Table 2 shows the roughness of $R_p x$ and $R_p y$ of the SLM specimen. Y is expressed in μm . Roughness $R_p x$ is presented in the second column, while $R_p y$ is presented in the final

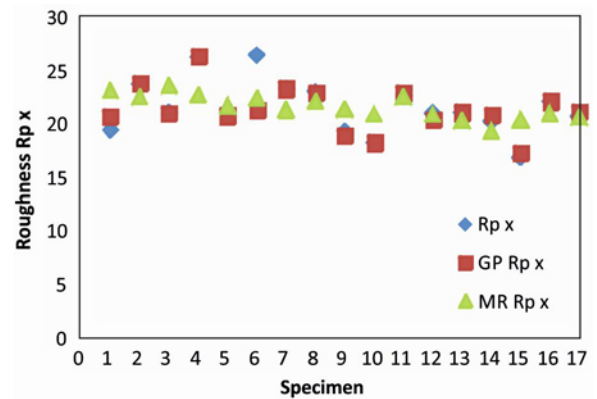


Fig. 9. Experimental and predicted data $R_p x$.

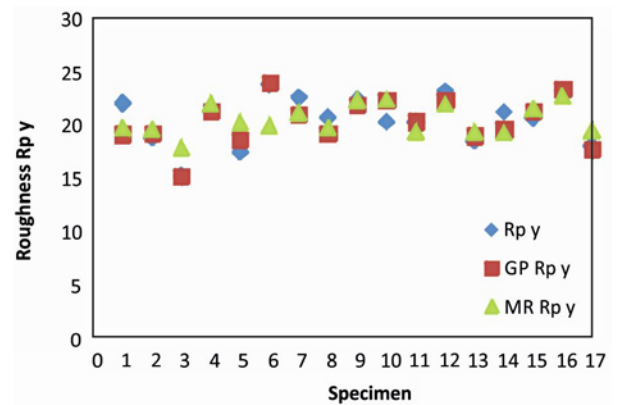


Fig. 10. Experimental and predicted data $R_p y$.

column. Specimen S6 has maximum roughness $R_p x$. Specimen S5 has minimum roughness $R_p y$. Specimen

Table 4. Prediction roughness $R_p x$ and $R_p y$ of SLM specimen with GP and MR

Specimen	GP $R_p x$	GP $R_p y$	MR $R_p x$	MR $R_p y$
S1	20.6195	19.0417	23.0	19.7
S2	23.7073	19.1161	22.4	19.5
S3	20.8691	15.1164	23.5	17.8
S4	26.2805	21.1524	22.6	22.0
S5	20.683	18.5083	21.6	20.2
S6	21.1949	23.8352	22.3	19.9
S7	23.1915	20.9413	21.2	21.1
S8	22.8615	19.0904	22.0	19.7
S9	18.7968	21.8041	21.3	22.3
S10	18.1566	22.2268	20.9	22.4
S11	22.7682	20.221	22.4	19.3
S12	20.3426	22.206	20.8	21.9
S13	20.9905	18.8635	20.2	19.3
S14	20.7718	19.4757	19.3	19.2
S15	17.1425	21.1723	20.3	21.5
S16	21.9916	23.2368	20.9	22.7
S17	21.0051	17.5792	20.5	19.4

S12 has maximum roughness $Ra Y$. Table 3 displays the genetic programming model for the roughness of $Rp y$ and $Rp x$ of the SLM specimen. The experimental and projected data, $Rp x$ and $Rp y$, are shown in Fig. 9 and Fig. 10, respectively.

Model of genetic programming for roughness $Rp x$ of SLM specimen presents Eq. (3). Model of genetic programming for roughness $Rp y$ of SLM specimen presents Eq. (4). Model of multiple regression for roughness $Rp x$ of SLM specimen presents Eq. (5). Model of multiple regression for roughness $Rp y$ of SLM specimen presents Eq. (6).

Model of genetic programming for roughness $Rp x$ of SLM specimen

$$\begin{aligned}
 Y = & \left(X2 \left(-21.6029 + 2X4 - X3^2(-X4 + X3X4) + \frac{X4}{4.68406 - \frac{X3^2}{X4} - X4 + 2X3(-X4 + X3X4)} \right) \right) / \\
 & \left(-17.0189 - X2 - 5.68406X3 + X4 + \frac{-X3 + \frac{X3^2}{X4} + X3X4}{X4} \right. \\
 & + X3 \left(X4 + \frac{X3 + X4}{X4^2(4.68406 + X3 - \frac{X3^2}{X4} - 2X4 + 2X3(-X4 + X3^2X4))} \right) \\
 & - \left(4.68406 - \frac{X3^2}{X4} \right) \left(-4.68406 - 2X3 + \frac{X3^2}{X4} + 2X4 + X3 \left(X4 + (2X3X4) / \left((-X4 + X3X4) \right. \right. \right. \\
 & \cdot \left. \left. \left. \left(4.68406 + X3 - \frac{X3^2}{X4} - 2X4 - \frac{-X3 + \frac{X3^2}{X4} + X3X4}{X4} + 2X3(-X4 + X3^2X4) \right) \right) \right) \right) \right) \\
 & + X3(X3 + X4) \left(-X4 + 2X3 \left(-2X4 + X3 \left(-X4 + X3(-X4 + X3^2)(-X4 + X3X4) \right. \right. \right. \\
 & \left. \left. \left. + \frac{2X3}{4.68406 + X3 - \frac{X3^2}{X4} - 2X4 + 2X3(-X4 + X3X4)} \right) \right) \right) \right). \tag{3}
 \end{aligned}$$

Model of genetic programming for roughness $Rp y$ of SLM specimen:

$$\begin{aligned}
 Y = & 7448 + X3 + \frac{X3}{2X4} - \frac{X2X4^3}{X1} - \frac{X4^2 \left(X2 + \frac{7.06492X2}{X1 \left(\frac{X3}{2X4} - 2X4 \right) X4} - \frac{17.1298X2 + X4}{X1X4} \right)}{X1} \\
 & + \frac{X1}{-8.06492 + X1 + 2X3 + 2X4 - \frac{X2^2X4^3}{X1} - \frac{X2X4^2}{-X1 + X4 + X1X4}}. \tag{4}
 \end{aligned}$$

Model of multiple regression for roughness $Rp X$ of SLM specimen:

$$Y = 7.025062107 + X1 \times 0.019486868 + X2 \times 0.000754866 + X3 \times 5.15784525 + X4 \times 0.86467551. \tag{5}$$

Model of multiple regression for roughness $Rp Y$ of SLM specimen:

$$Y = 20.9026845 + X1 \times 0.008218161 - X2 \times 0.001986141 + X3 \times 2.897586093 - X4 \times 8.871867038. \tag{6}$$

Regression statistics $R_p x$		ANOVA $R_p x$					
Multiple R	0.439025						
R Square	0.192743						
Adjusted R Square	−0.07634						
Standard error	2.651702						
Observations	17						
		df	SS	MS	F	Significance F	
		Regression	4	20.1464	5.036599	0.716288	0.596777017
		Residual	12	84.37831	7.031526		
		Total	16	104.5247			

Regression statistics $R_p x$				
	Coefficients	Standard error	t stat	P -value
Intercept	7.025062107	12.52450812	0.560905	0.585184
Power	0.019486868	0.014926675	1.305506	0.216196
Speed	0.000754866	0.003618846	0.208593	0.838265
Fractal dimension	5.15784525	6.123828793	0.842258	0.416114
Density of network	0.86467551	4.284879574	0.201797	0.843456

Regression statistics $R_p y$		ANOVA $R_p y$					
Multiple R	0.619158						
R Square	0.383357						
Adjusted R Square	0.177809						
Standard error	2.110325						
Observations	17						
		df	SS	MS	F	Significance F	
		Regression	4	33.22382	8.305954	1.865051	0.181441126
		Residual	12	53.44167	4.453473		
		Total	16	86.66549			

Regression statistics $R_p y$				
	Coefficients	Standard error	t stat	P -value
Intercept	20.9026845	9.9674783	2.097089	0.057843
Power	0.008218161	0.011879214	0.69181	0.502223
Speed	−0.001986141	0.002880015	−0.68963	0.503546
Fractal dimension	2.897586093	4.873575075	0.59455	0.563186
Density of network	−8.871867038	3.410069582	−2.60167	0.023155

The increased development of flaws in the SLM process is one of its main drawbacks. Defect generation in SLM parts may result from incorrectly selecting one or more parameters. By forming a point of stress concentration and initiating and propagating fatigue cracks, these surface imperfections can significantly reduce the overall strength and performance of the SLM part. More often than not, surface roughness is even more harmful than the typical material flaws made using additive manufacturing [14]. Yasa et al.'s study [15] examined how precision forging and various machining techniques were compared to selective laser melting (SLM) for producing parts with surface finishing. The surface roughness and oxidation levels of the SLM parts were discovered to be higher than those of the other methods by the authors. The roughness levels were observed to range from 10 to 15 μm . A kind of SLM called MicroSLM, which uses finer powder particles and a smaller laser spot size, may lessen the surface roughness and oxidation problems noted by Yasa et al. [15]. MicroSLM can create items with smoother surfaces and finer details using smaller laser spot sizes,

which reduces surface roughness [16]. Additionally, finer powder particles can be used with microSLM, which lowers the part's oxidation levels by minimizing residual stress and flaws. The surface quality of the SLM components is enhanced by adequately selecting the processing variables. The process parameters influencing the surface quality of SLM-built components are scanning speed and laser power. ANOVA statistical analysis and regression statistics were applied to evaluate the factors influencing the surface roughness, $R_p x$ and $R_p y$. Kaynak and Tascioglu [17] confirmed that a lower surface finish is obtained in the SLM process, partly due to partially melted powders and defects like pores and cavities on surfaces of SLM parts, even though the roughness depends on process parameters like scanning speeds and the temperature of the SLM part surface [18]. Nevertheless, some additional variables and factors affect surface roughness. The size of the metallic powder, wall angle, liquid metal pool, and layer thickness are more important than the others [19], where a particular surface's wall angle or draft angle is measured horizontally.

4. Conclusions

In this article, modeling the roughness surface of the SLM specimen is presented. Over the past twenty years, metallic alloy additive manufacturing (AM) has been popular across various industries and has garnered significant interest from the academic community. The production of value-added parts – which traditional processing methods cannot produce – and the reduced waste (increased buy-to-fly ratio) of additive manufacturing (AM) are the main drivers of this trend. Fine metal powder is the initial material used in the SLM process, and it is placed in extremely thin layers (0.05–0.12 mm). A high-precision laser scans the component contour after each layer, and the powder is melted by the precisely timed energy input. The next layer of metal powder is added after the laser has completely covered the surface and the building platform has been lowered by precisely one layer thickness. This procedure is then carried out once more until every component has been laser-printed three-dimensionally, layer by layer. Depending on the size of the installation location, the complete selective laser melting building process may take several hours.

Laser beam melting is an additive manufacturing process in which components are manufactured layer by layer from powdery material. The SLM process does not differ fundamentally from the SLS process. However, unlike selective laser sintering (SLS), the material powder is not sintered in selective laser melting (SLM). In the SLM process, the material powder is locally melted directly at the processing point using the thermal energy of a laser beam. The installation space with the powder material is heated to just below the melting temperature. The working space is usually filled with a protective gas to prevent the material from oxidizing. Due to the large temperature difference between the youngest component level and the already cooled layers, if the process is carried out incorrectly, undesirable effects can occur, such as warping of the component, burns, and so-called curling, a bending of the component edges. The workpieces are firmly welded to the base plate using a support structure to avoid this. This support structure must later be removed manually. Selective laser melting is a resource-saving process that produces little waste because the excess material can be processed through sieving and largely reused. With selective laser melting (SLM), the physical 3D object is produced by melting a metallic powder. The 3D data set is cut into individual layers and built up according to the contours of the digital file. The process is complex and, therefore, takes several working days.

The technology of direct supply of energy and material has become widespread in various manufacturing industries and beyond. It is more than just 3D printing. It performs various production tasks, ranging

from coating and repairing components to the complex production of blanks and parts. It is most widely used in the aviation industry, aerospace industry, mechanical engineering, shipbuilding, medicine, dentistry, energy, petrochemical industry, construction of buildings and structures, production of souvenirs, advertising industry, etc. Laser surfacing is also used when repairing expensive workpieces. This is relevant for products made of special nickel alloys. At their price, repairing the part is more profitable than buying a new one. Due to the high work precision and minimal thermal load, the reproducibility will be much higher than that of classical brewing methods.

Unlike traditional material removal methods, rapid prototyping technologies aim to create complex products by sequentially adding material(s). Many rapid prototyping methods are known, and they differ in the material used and the method of shaping the product. An innovative method for selective laser melting of a physical replica of various objects made of metals, alloys, and metal matrix composite materials to meet the requirements of the aerospace, defense, automotive, and biomedical industries. An important direction in developing selective laser melting technology is to improve the quality of the formed product. This is a complex multi-parameter process in which about 130 parameters can be identified that influence the final result.

References

- [1] Q. Wei, H. Li, G. Liu, Y. He, Y. Wang, Y. E. Tan, D. Wang, X. Peng, G. Yang, N. Tsubaki, Metal 3D printing technology for functional integration of the catalytic system, *Nat. Commun.* 11 (2020) 4098. <https://doi.org/10.1038/s41467-020-17941-8>
- [2] P. Jamshidi, M. Aristizabal, W. Kong, V. Villapun, S. C. Cox, L. M. Grover, M. M. Attallah, Selective laser melting of Ti-6Al-4V: The impact of post-processing on the tensile, fatigue and biological properties for medical implant applications, *Materials* 13 (2020) 2813. <https://doi.org/10.3390/ma13122813>
- [3] B. B. Mandelbrot, *The Fractal Geometry of Nature*. Times Books, 1982. Retrieved from <https://www.amazon-Geometry-Nature-Benoit-Mandelbrot/dp/0716711869>
- [4] M. Z. Al-Taie, S. Kadry, Information Diffusion in Social Networks. In: *Python for Graph and Network Analysis*. Advanced Information and Knowledge Processing. Springer, Cham. (2017) pp. 165–184. https://doi.org/10.1007/978-3-319-53004-8_8
- [5] S. Sarangi, Md. Sahidullah, G. Saha, Optimization of data-driven filter bank for automatic speaker verification, *Digital Signal Processing* 104 (2020) 102795. <https://doi.org/10.1016/j.dsp.2020.102795>
- [6] EOS from <https://www.eos.info/de>
- [7] C. Zhai, Y. Gan, D. Hanaor, G. Proust, D. Re-traint, The role of surface structure in normal contact

- stiffness, *Experimental Mechanics* 56 (2016) 359–368. <http://dx.doi.org/10.1007/s11340-015-0107-0>
- [8] A. R. Durmaz, M. Müller, B. Lei, A. Thomas, D. Britz, E. A. Holm, Ch. Eberl, F. Mücklich, P. Gumbsch, A deep learning approach for complex microstructure inference, *Nat. Commun.* 12 (2021) 6272. <https://doi.org/10.1038/s41467-021-26565-5>
- [9] H. Porchon, Fractal topology foundations, *Topology and its Applications* 159 (2012) 3156–3170. <https://doi.org/10.1016/j.topol.2012.06.007>
- [10] M. Kovačič, U. Župerl, Continuous caster final electromagnetic stirrers position optimization using genetic programming, *Materials and Manufacturing Processes* 38 (2023) 2009–2017. <https://doi.org/10.1080/10426914.2023.2219317>
- [11] M. Kovačič, U. Župerl, M. Brezočnik, Optimization of the rhomboidity of continuously cast billets using linear regression and genetic programming: A real industrial study, *Advances in Production Engineering & Management* 17 (2022) 469–478. <https://doi.org/10.14743/apem2022.4.449>
- [12] M. Kovačič, U. Župerl, Modeling of tensile test results for low alloy steels by linear regression and genetic programming taking into account the non-metallic inclusions, *Metals* 12 (2022) 1343–1343. <https://doi.org/10.3390/met12081343>
- [13] T. A. Trunfio, A. Scala, C. Giglio, G. Rossi, A. Borrelli, M. Romano, G. Improta, Multiple regression model to analyze the total LOS for patients undergoing laparoscopic appendectomy, *BMC Med. Inform. Decis. Mak.* 22 (2022) 141. <https://doi.org/10.1186/s12911-022-01884-9>
- [14] H. Masuo, Y. Tanaka, S. Morokoshi, H. Yagura, T. Uchida, Y. Yamamoto, Y. Murakami, Effects of defects, surface roughness and HIP on fatigue strength of Ti-6Al-4V manufactured by additive manufacturing, *Procedia Struct. Integr.* 7 (2017) 19–26. <https://doi.org/10.1016/j.prostr.2017.11.055>
- [15] E. Yasa, J. Deckers, J. Kruth, The investigation of the influence of laser re-melting on density, surface quality and microstructure of selective laser melting parts, *Rapid Prototyp. J.* 17 (2011) 312–327. <https://doi.org/10.1108/13552541111156450>
- [16] B. Nagarajan, Z. Hu, X. Song, W. Zhai, J. Wei, Development of micro selective laser melting: The state of the art and future perspectives, *Engineering* 5 (2019) 702–720. <https://doi.org/10.1016/J.ENG.2019.07.002>
- [17] Y. Kaynak, E. Tascioglu, Post-processing effects on the surface characteristics of Inconel 718 alloy fabricated by selective laser melting additive manufacturing, *Prog. Addit. Manuf.* 5 (2020) 221–234. <https://doi.org/10.1007/s40964-019-00099-1>
- [18] I. Koutiri, E. Pessard, P. Peyre, O. Amlou, T. De Terris, Influence of SLM process parameters on the surface finish, porosity rate and fatigue, *Journal of Materials Processing Technology* 255 (2018) 536–546. <https://doi.org/10.1016/J.JMATPROTEC.2017.12.043>
- [19] L. Masseling, Reduction of surface roughness of SLM components by means of modulated laser, *Annu. Rep.* 69572 (2015).